P7.2 CHARACTERIZATION OF THE ERROR STRUCTURE OF PRECIPITATION NOWCASTING

Jordi Roca-Sancho*[1], Marc Berenguer[2], Isztar Zawadzki[2], Daniel Sempere-Torres[1]

[1]Centre de Recerca Aplicada en Hidrometeorologia. Universitat Politècnica de Catalunya, Barcelona (Spain).

[2]J.S. Marshall Radar Observatory, Department of Atmospheric and Oceanic Sciences, McGill University, Montreal, Quebec (Canada).

1. INTRODUCTION

Radar-based extrapolation techniques have shown certain skill in rainfall nowcasting. However, precipitation growth and decay not explained by motion are the main source of forecasting error together, in a minor extent, with the estimation of the motion field (Germann et al. 2006). Simiarly as done for radar QPE (Lee et al. 2007; Germann et al. 2009), an ensemble-based probabilistic approach could be useful to describe the uncertainty in very short term QPF. In this sense, first attempts have been carried out by Bowler et al. (2006) and Berenguer et al. (2006). All these methodologies require a detailed analysis of the structure of the errors affecting the forecasts of precipitation, similarly as done by Ciach et al. (2007) and Berenguer and Zawadzki (2008) for radar rainfall estimates.

The main goal of this work is to provide a complete description of the structure of the errors affecting the nowcasts produced by MAPLE (the McGill Algorithm for Precipitation nowcasting by Lagrangian Extrapolation; Laroche and Zawadzki 1995; Germann and Zawadzki 2002) over Central and East United States. The analysis includes the statistical distribution of the errors,, and the correlation in space and time, also the dependence on factors as the location, time of the day or the season are taken into account.

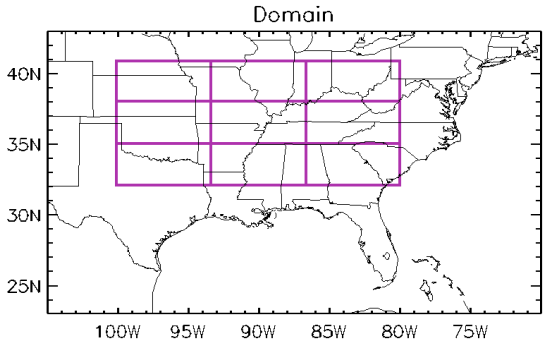

Figure 1.Domain and nine subdomains where the anakysis has been carried out.

2. DATA USED IN THIS STUDY

MAPLE has been run using reflectivity mosaics corresponding to the 2.5 km CAPPI maps from the 3D composites generated by the National Severe Storms Laboratory (NSSL) over United States. The analysis has been carried out during two periods in 2008 (16 April to 06 June, and 1 to 31 July 2008) and over the domain 32-41N and 80-100W, which has been subdivided in 9 subdomains as shown in Figure 1 (from North to South and from West to East, NW, N, NE, W, C, E, SW, S, SE). MAPLE forecasts for every hour of the day have been compared offlline against actually observed radar reflectivity mosaics to obtain the error in the forecast.

Both observed and forecasted fields are converted from reflectivity mosaics (Z) to rain rate fields (R) through a standard relationship, $Z=300R^{1.5}$.

3. CHARACTERIZATION OF THE ERROR STRUCTURE

3.1 Definition of the residual fields

We have quantified the error in MAPLE forecasts using series of residual fields. Given a forecasted rainfall field and the actual observation at the verification time we define the residual field at a given point as the difference between the forecast and the observation, provided that there is rainfall in that point either in the observation or in the forecast. Thus, the residual includes hits, misses and false alarms (see an example in Figure 2).

3.2 Statistical distribution

The residuals' statistical distribution is generally symmetrical and unbiased for spring and summer (shown in Figure 3, graphics for regions are collocated with the grid above). The shape of the distribution is repeated for every region and lead time. In spring the distribution in Western regions (NW, W, SW) are slightly biased indicating general underestimation, this is due to the precipitation systems initiated near the Rocky Mountains which are less predictable in spring than in summer.

3.3 Diurnal evolution of the bias

Growth and decay associated to the diurnal cycle of precipitation (see e.g. Carbone et al. 2002) cannot be reproduced by MAPLE. Figure 4 (on the left) shows the residuals' diurnal cycle in relation to the cycle in observation and forecast for the spring period. Focusing on the C and S subdomains is evident that actual peaks of precipitation area (observation) have been reproduced and moved forward a lag of 4 hours –which is the lead time of this example- in the forecast (showing the inability of MAPLE to account for diurnal evolution).

On the right of Figure 4 there is the mean rainfall as a function of the time of the day for observations and MAPLE forecasts. This mean is conditioned to the presence of precipitation either in observation or in the forecast. In NW and W subdomains is obvious the underestimation mentioned above. The semi-diurnal cycle of the observed mean rainfall in the SE region is only apparent as well as the moved cycle in the forecasted mean. The low occurrence of precipitation in the SE region during the spring period

analysed allow that a single day with large scale system dominates the average as a function of the time of the day, producing the effect of a semi-diurnal cycle.

Figure 5 shows the same as Figure 4 for the summer period. In summer the diurnal cycle is stronger than in spring and the forecasted cycle more evident (for both coverage and mean rainfall), especially in the S and SE subdomains.

Figure 6 shows the mean error as a function of the time of the day which is exactly the difference between the mean rainfall of the forecast and the one of the observation showed above (only for the lead time of 4h, Figure 4 and 5 on the right). In spring (on the left) underestimation in Western regions (NW, W, SW) is high around 01h UTC (as shown in Figure 4 right). In NE, E, and S regions the mean error do not seem to depend on the time of the day and in the SE subdomain an artificial semi-diurnal cycle is inherited from the mentioned apparent semi-diurnal cycle of mean rainfall.

In summer (Figure 6 on the right) the diurnal cycle of the mean error is clearer than in spring (especially in the S and SE regions) because of the regularity of the diurnal cycle of precipitation in this season. In the SW subdomain a semi-diurnal cycle of mean precipitation is reproduced in the residuals.

3.4 Standard deviation

The standard deviation of the residuals, which is roughly the root mean square error (RMSE) of the forecasts, is shown in Figure 7 as a function of the time of the day. Standard deviation has its own diurnal patterns which are evident in the West in spring (apparent semi-diurnal evolution in SE) and generally clear in summer.

There are differences in the standard deviation among regions. In spring Western regions (NW, W, SW) show a high standard deviation because of the initiation of precipitation near the Rocky Mountains is less stable and so less predictable. On the other hand, in summer the highest variance occurs in the N and C subdomains. An explanation is that in summer the eastward propagation of precipitation ceases about 95W instead of 88W in spring (Surcel et al. 2009).

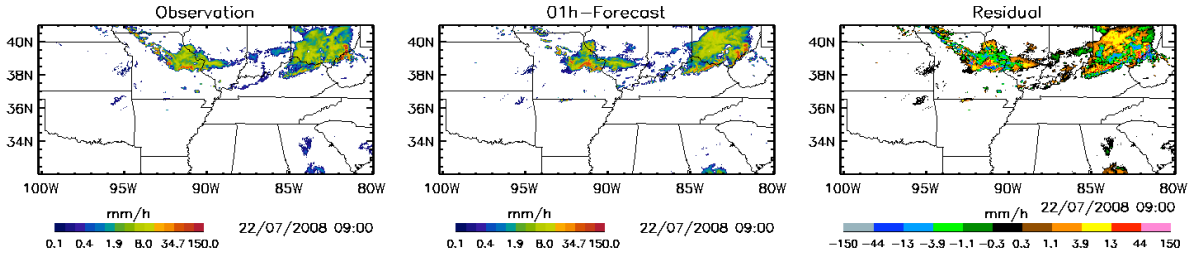

Figure 2. Example of residual field with the corresponding observed and forecasted field.

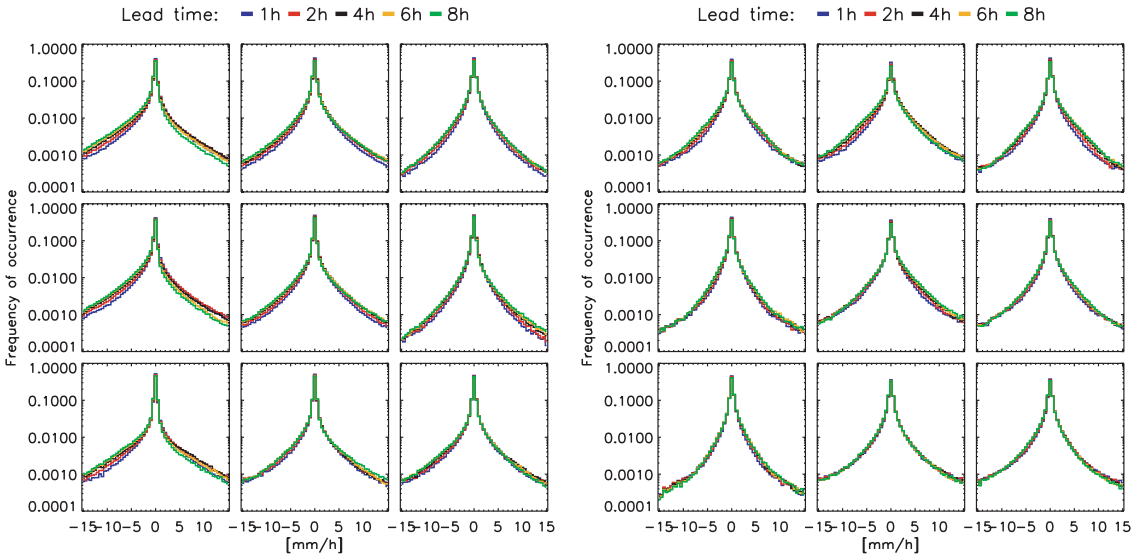

Figure 3.Statistical distribution of the residuals for each subdomain (collocated as in Figure 1) and lead time in spring (left) and summer (right).

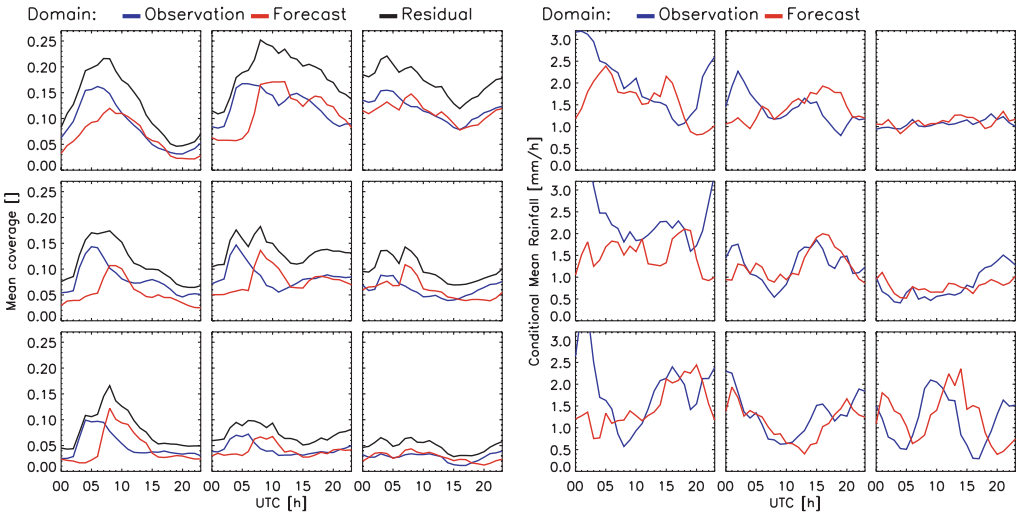

Figure 4. On the left, evolution of the mean coverage of the fields (observation, forecast and residual) as a function of the time of the day for a lead time of 4 hours in the spring period. On the right evolution of the mean rainfall conditional to the existence of the residual, that is, to the presence of either observed or forecasted precipitation, for the same period.

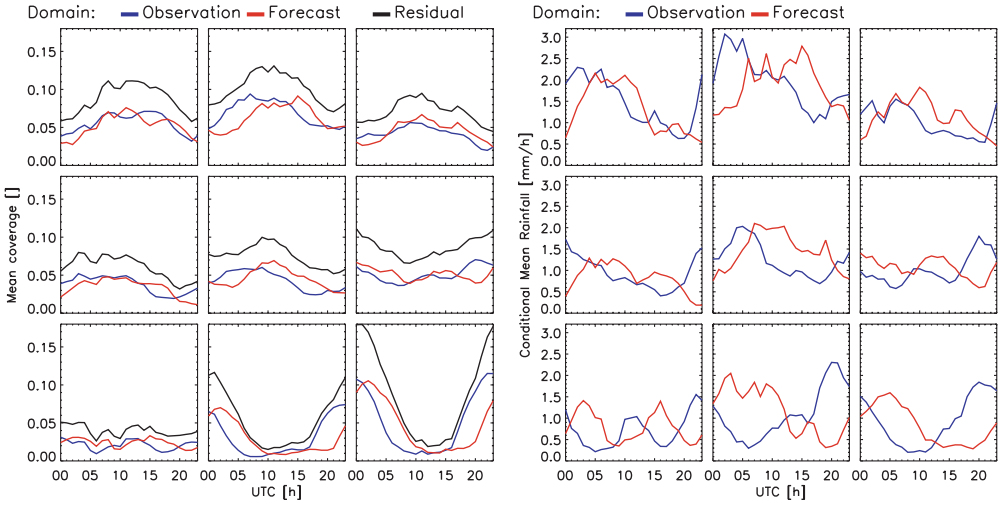

Figure 5. On the left, evolution of the mean coverage of the fields (observation, forecast and residual) as a function of the time of the day for a lead time of 4 hours in the summer period. On the right evolution of the mean rainfall conditional to the existence of the residual, that is, to the presence of either observed or forecasted precipitation, for the same period

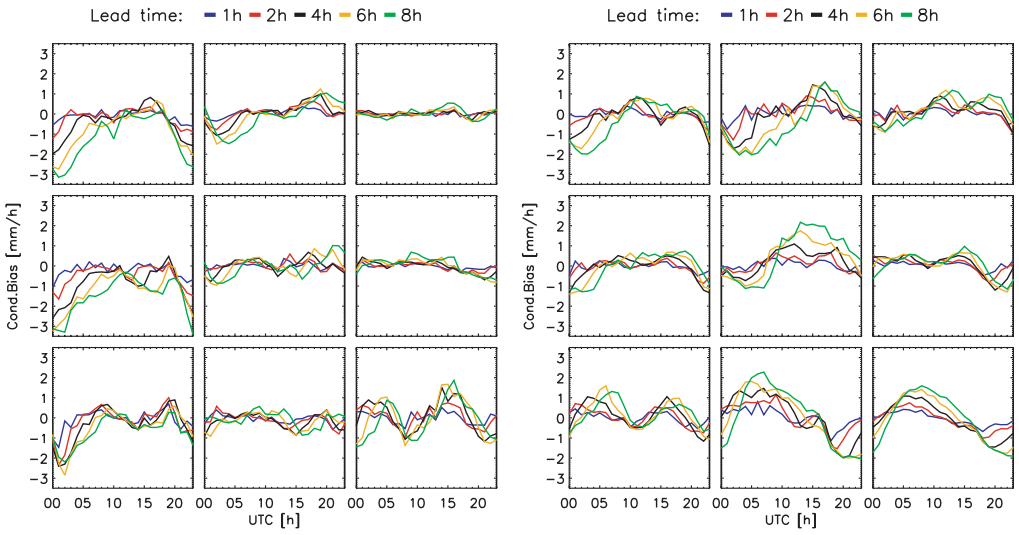

Figure 6. Evolution of the bias as a function of time of day for each region (collocated as in Figure 1) and for each lead time referred to the spring period on the left and to the summer period on the right.

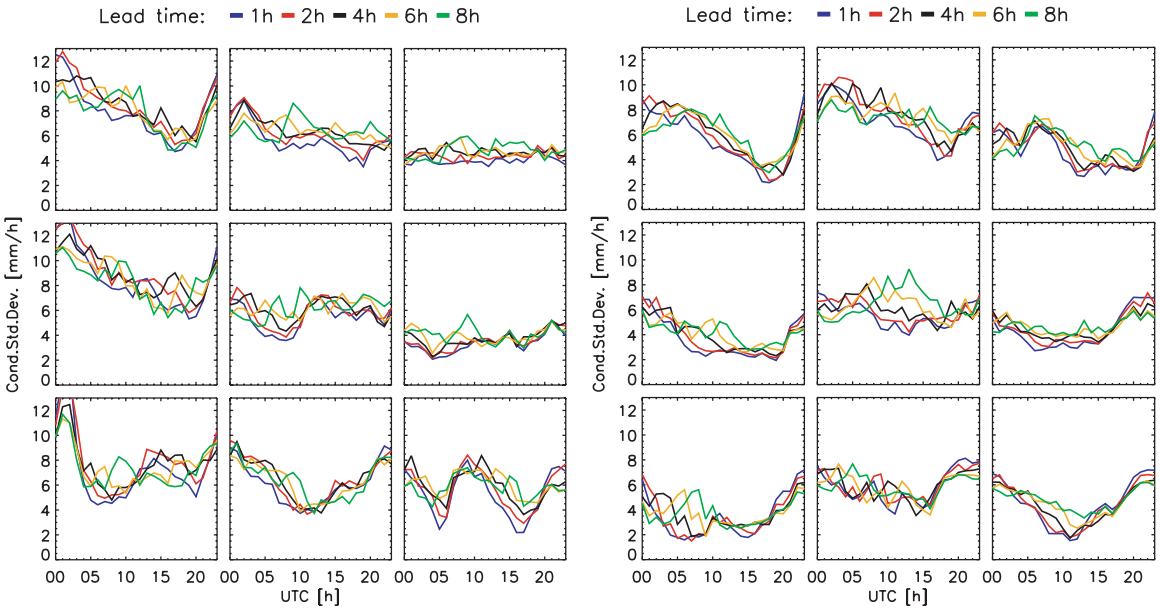

Figure 7. Evolution of the standard deviation as a function of time of day for each region (collocated as in Figure 1) and for each lead time referred to the spring period on the left and to the summer period on the right.

3.5 Scale analysis

The Haar wavelet spectrum of a residual field relates each scale of precipitation to its contribution to the variance of the field.

Figure 8 shows the normalized wavelet spectra for each region and lead times of 1, 2 and 4 hours for both analyzed periods (spring and summer). We can see that in the S, SE, E, subdomains the smallest scale (10 km) is significantly more dominant than the rest for both seasons, while the scales of 10 and 20 km have a similar relevance over the NW (spring) and the N (summer) regions. This is due to type of precipitation usual in the different regions. In the South small scales are dominant because convective rains are frequent in these regions. On the other hand, stratiform rain is more frequent in the North, which entails an enhancement of larger scales. For longer lead times, the error fields show more large scale patterns. This is in a good part due to the increase in the number of misses and false alarms as the lead time increases, which results in errors showing patterns that resemble those of the precipitation fields themselves.

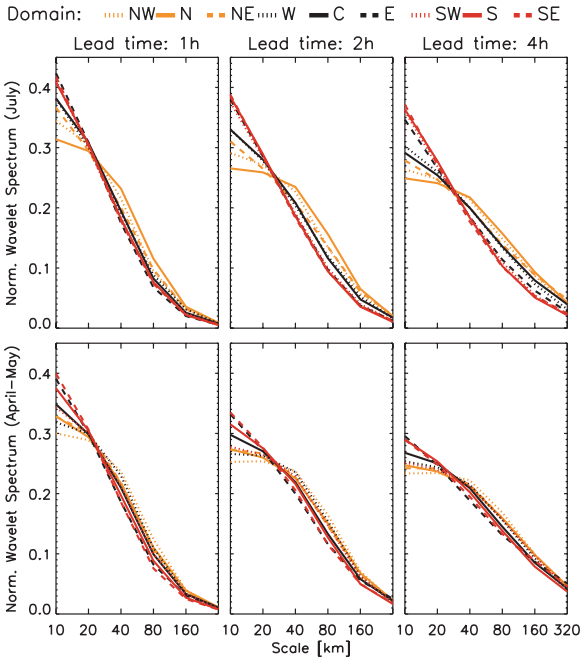

Figure 8. Normalized wavelet spectrum of the residual fields for each region (9 lines), season (spring at the bottom and summer in the top) and three lead times (3 columns).

3.6 Temporal autocorrelation in Eulerian coordinates

Figure 9 shows that there is no temporal correlation in the residuals fields for the lead times of 1 and 2 hours and low correlation for higher lead times. That is for a fix coordinate system. To fully describe the temporal variation of the error field, it would also be necessary to describe the auto-correlation of the error fields in a coordinate system moving together with the precipitation

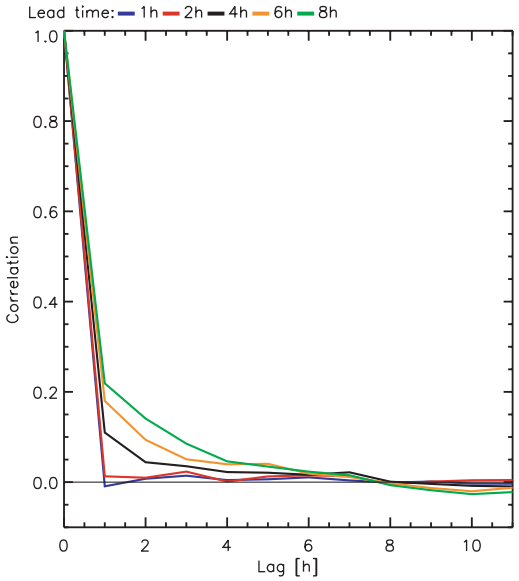

Figure 9. Autocorrelation function for each lead time.

4. CONCLUSION

A complete statistical analysis of the error in MAPLE forecasts has been carried out comparing periods from spring and summer 2008. The diurnal cycle of precipitation that cannot be forecasted by MAPLE is clearly reproduced in the residuals in summer and in the SW domain a semi-diurnal component is noticed. In spring the signal is only clear in the NW, N and SW regions. In the SE there is a false semi-diurnal cycle. The 10 km scale is the most relevant in the error fields in the Northern regions while in the southern regions both 10 and 20 km scale have similar weight. Residual fields have a very low temporal correlation in Eulerian coordinates. A next step to fully describe the temporal evolution of the errors is to investigate it in moving coordinates.

An ultimate goal of this analysis is the statistical simulation of series of residual fields, and so the generation of ensembles of rainfall forecasts.

Acknowledgements: This work has been carried out in the framework of the EC project IMPRINTS (FP7-ENV-2008-1-226555). Thanks are due to the Catalan Water Agency (ACA) for financial support. The first author is also grateful to the Spanish Science and Innovation Ministry for the FPI scholarship BES-2008-005217 associated to the project ESP2007-62417.

References

Berenguer, M., and I. Zawadzki, 2008: A Study of the Error Covariance Matrix of Radar Rainfall Estimates in Stratiform Rain. *Weather and Forecasting*, **23,** 1085-1101.

Bowler, N. E., C. E. Pierce, and A. W. Seed, 2006: STEPS: A probabilistic precipitation forecasting scheme which merges an extrapolation nowcast with downscaled NWP. *Quarterly Journal of the Royal Meteorological Society*, **132,** 2127-2155.

Carbone, R. E., J. D. Tuttle, D. A. Ahijevych, and S. B. Trier, 2002: Inferences of Predictability Associated with Warm Season Precipitation Episodes. *Journal of the Atmospheric Sciences*, **59,** 2033-2056.

Ciach, G. J., W. F. Krajewski, and G. Villarini, 2007: Product-Error-Driven Uncertainty Model for Probabilistic Quantitative Precipitation Estimation with NEXRAD Data. *Journal of Hydrometeorology*, **8,** 1325-1347.

Germann, U., and I. Zawadzki, 2002: Scale-Dependence of the Predictability of Precipitation from Continental Radar Images. Part I: Description of the Methodology. *Monthly Weather Review*, **130,** 2859-2873.

Germann, U., I. Zawadzki, and B. Turner, 2006: Predictability of Precipitation from Continental Radar Images. Part IV: Limits to Prediction. *Journal of the Atmospheric Sciences*, **63,** 2092-2108.

Germann, U., M. Berenguer, D. Sempere-Torres, and M. Zappa, 2009: REAL - Ensemble radar precipitation estimation for hydrology in a mountainous region. *Quarterly Journal of the Royal Meteorological Society*, **135,** 445-456.

Laroche, S., and I. Zawadzki, 1995: Retrievals of Horizontal Winds from Single-Doppler Clear-Air Data by Methods of Cross Correlation and Variational Analysis. *Journal of Atmospheric and Oceanic Technology*, **12,** 721-738.

Lee, G., A. W. Seed, and I. Zawadzki, 2007: Modeling the Variability of Drop Size Distributions in Space and Time. *Journal of Applied Meteorology and Climatology*, **46,** 742-756.

Surcel M., M. Berenguer, and I. Zawadzki, 2009: The diurnal cycle of precipitation from continental radar images and numerical weather prediction models. Part I: Methodology and Seasonal Comparison. *Monthly Weather Review* (Submitted)